International Journal of Nanoelectronics and Materials
Volume 13 (Special Issue) Dec 2020 [83-90]

Theoretical Demonstration of Elastic Wave Guiding in a Pillar-Based Phononic Crystal Slab

Mohd Syafiq Faiz[1], Kim S. Siow[1], MF Mohd Razip Wee[1], Muhammad Musoddiq Jaafar[1,2], Burhanuddin Yeop Majlis[1] and Ahmad Rifqi Md. Zain[1,3*]

[1]*Institute of Microengineering and Nanoelectronics (IMEN), Level 4, Research Complex, Universiti Kebangsaan Malaysia, 43600 Bangi, Selangor, Malaysia.*
[2]*International College of Semiconductor Technology, National Chiao Tung University, University Road, Hsinchu 30010, Taiwan, ROC.*
[3]*School of Engineering and Applied Science (SEAS), Harvard University, John A. Paulson building, 31 Oxford St, Cambridge 02138, United States.*

ABSTRACT

We demonstrated theoretically the wave guiding of elastics waves in a two-dimensional (2D) phononic crystal (PnC) slab. The simulation model based on the Finite Element Method (FEM) was used to calculate the dispersion relation of unit cells that shows a complete band gap between frequency, f=312–412 kHz. The supercell technique to simulate two waveguides size shows filtering frequencies between 365-397 kHz within the band gap. We discuss the frequency shift of the wave guide as a function of the defect size for the possibility of elastic wave filtering application. `

Keywords: Lamb Waves, Phononic Crystal Slabs, Phononic Waveguiding.

1. INTRODUCTION

Phononic Crystal (PnC) is an artificial periodic inclusion with spatial modulation of elastic constant embedded in a matrix background. Lately, this novel crystal has attracted much attention due to its important property namely phononic crystal band gap (PnBg) which defined as the region of frequency range where no mechanical energy can propagate in any polarization. The phenomena are the result of destructive interference of the scattered acoustics/elastics wave by the inclusion elements and strongly depends on several crucial factors such as the high contrast of inclusion and matrix physical properties [1-3], the geometry of inclusions and the filling factor [4,5]. Such systems offers a plethora of potential application in elastic or acoustic wave studies such as vibration or noise filtering, acoustic/elastic waveguiding, demuliplexing, and many more [6-11].

A defect inside the crystal structure can offer many applications, for example as resonator (for energy storage elements) and wave guiding (for filters and delay lines) [12, 13]. For instance, Mohammadi *et al*., [14] studied a resonator in PnC slab by creating a line defect in hexagonal hole structure made from silicon. Oudich *et al*., [15] used slab structure to demonstrate a straight waveguide for solid-solid stubbed-based PnC plate. Vasseur et al., [16] studied the waveguide for hole-based plate structure with respect to the variation width of the waveguide. In this case, the *Lamb*-waves propagation in slab-based waveguide offer more advantages over semi-infinite media because it shows a higher confinement of wave energy [17, 18] compared to surface acoustic wave (SAW) that endure the coupling issue between the SAW and the bulk. The ability to confine the energy in a more excellent manner than SAW makes PnC slab an excellent choice for waveguiding. Other than low loss issue, PnC slab is also compatible with standard MEMS

*Corresponding author: *rifqi@ukm.edu.my*

technology and CMOS fabrication [19]. Even though the fabrication for PnC slab is more challenging than SAW-based PnC, it has its merits and better confinement for elastic wave which make the PnC slab a better choice for high-performance devices.

Lamb waves represent a category of Guided Wave (GW) that consists of two fundamental modes, which is the symmetric and antisymmetric that produced in the components of plates and shells. With distinctive propagation characteristics, the waves have gained an increasing preference for both damage identification and the wave guiding. Since the stress for the elastic disturbance of the Lamb wave take the entire thickness, the plate structure can be interrogated for both at the surface and internal defects. In the perspective of wave guiding, the *Lamb* wave is a superior candidate due to its various benefit of its wave confinement. The presence study focused on the theoretical study for the PnC waveguide in line defects based on piezoelectric materials. In this study, we proposed a Lithium Niobate, $LiNBO_3$ in order to excite the *Lamb* mode through the presence of interdigital transducers (IDTs) fabricated using lithography technique. We added a periodic array of Nickel pillar to act as resonator on top of the slab structure.

The paper is organized as the following. Firstly, we calculated the position of band gap by using the unit cell structure consisting of periodic pillars arranged in a square array on the top of the slab. Next, the detail evolution of this bandgap with respect to geometrical criterion and the nature of the band gap are discussed. Finally, we demonstrate the possibility to confine energy by introducing linear defect to the structure to act as a selective waveguide.

2. MATERIALS AND METHODS

The proposed structure in this study is schematically shown in Fig. 1 (a). A pillar made of nickel, with radius r, height of pillar h_p, and lattice constant a, is deposited on lithium niobate slab with thickness of h in a square lattice arrangement. Details of materials properties are listed in Table 1.

Table 1 Material constant of Y-128 lithium niobate, $LiNBO_3$ and nickel, Ni

Material	Mass density (Kg/m^3)	Elastic constant (10^{10} N/m^2)					
		C_{11}	C_{12}	C_{13}	C_{33}	C_{44}	$-C_{14}$
Lithium Niobate	4.62	1.98	5.35	6.63	1.86	7.50	6.95
Nickel	0.89	0.27	0.17	0.17		0.12	

We calculate the band diagram by using Finite Element Method (FEM) based on COMSOL Mutltiphysics 3.5a. By using *Bloch Floquet* theorem, the unit cells in Fig.1(a) is repeated periodically and assumed to be infinite in x and y-directions while the z-direction (a perpendicular direction to slab surface) is assumed to be finite. By changing the value k in the first irreducible *Brillouin* zone, the FEM algorithm is able to solve the eigenvalue problem and obtain the dispersion relation. The propagation of waves in a periodic media with lattice constant a must satisfy the following equation [20]:

$$U_i(x+a\oplus m,y,z) = u_i(x,y,z)e^{-i(ak_x m)}e^{-i(ak_y m)} \quad (1)$$

Where k_x, and k_y are *Bloch* wave vectors components in x and y directions. While u_i is the displacement with i=x, y and z. By assuming a uniform mechanical and electrical field with time dependence exp (jt) where ω is the angular frequency, the piezoelectric with no external applied force is given by [20]:

$$[K_{uu} - \omega^2 M_{uu}\ K_{u\phi}\ K_{\phi u}\ K_{\phi\phi}\ ](u\ \phi\ ) = (0\ 0\ ) \quad (2)$$

Where K_{uu}, M_{uu}, u, ϕ are the stiffness, mass matrices of elastic part, displacement and electrical potential at the point of mesh in a vector form respectively. While $k_{u\phi}$ and $K_{\phi u}$, are piezoelectric coupling matrices, and $K_{\phi\phi}$ accounts for the dielectric. The frequency, f as function of wave vector, k ($ka/2\pi$) is calculated based on this method.

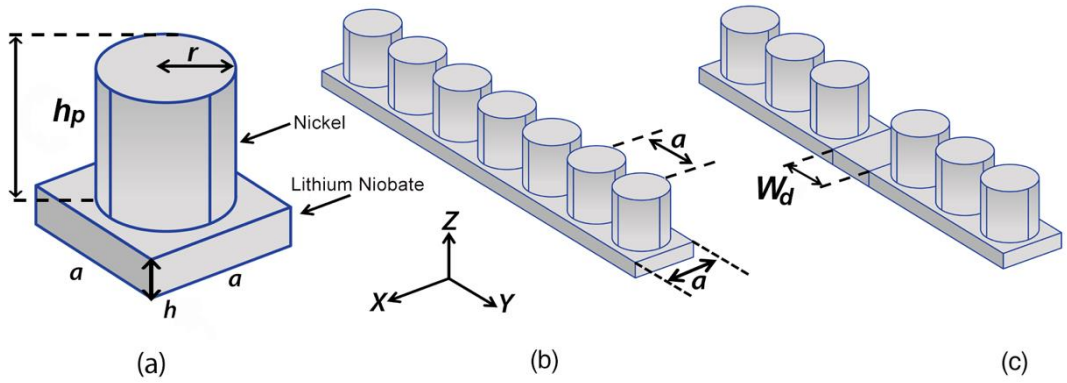

Figure 1. (a) Schematic of unit cell for phononic crystal slab used in simulation. (b) the schematic for1x7 perfect super cell and (c) super cell with linear defect, W_d.

In order to calculate the effect of waveguide, we study the phenomena based on the supercell technique. Figs. 1 (b) shows a perfect supercell model to calculate the band diagram in the ΓX direction. A defect, W_d introduced in this structure will give rise to localized mode inside the band region that enable the possibility for waveguide - Figs. 1 (c).

To calculate the transmission spectrum and their respective surface displacement, Fig. 2 shows the 7 finite periods of unit cells in the *x*-direction and infinite periods in the *y*-direction used in our numerical study. To avoid any energy reflection from incoming waves, we use perfectly matched layer (PML) technique in the *x*-direction of wave propagation. To apply this absorbing area, the governing equation is written as [22]

$$\frac{1}{\gamma}\frac{\partial T_{ij}}{\partial x_j} = -\rho\omega^2 u_i \quad (3)$$

where ρ is the density of material, T_{ij} is the mechanical stress, ω is the angular frequency, γ_j is an artificial damping at position x_j and is given by the following relation [22]

$$\gamma_x(x) = 1 - i\sigma_x(x - x_l)^2 \quad (4)$$

Where x_l is the coordinate at the beginning of PML and σ_x is fixed according to the level of attenuation of PML space.

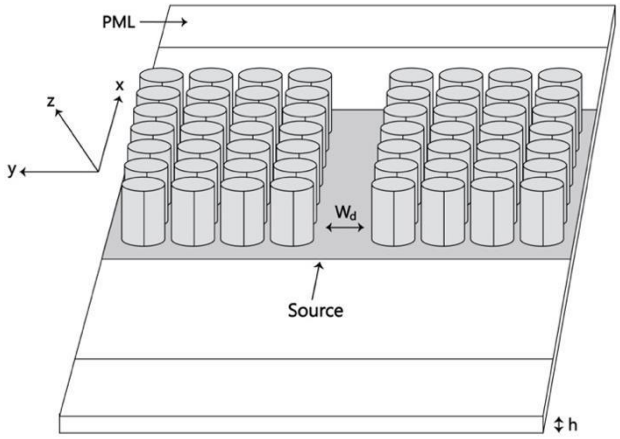

Figure 2. Finite model of phononic crystal slab waveguide with the PML region implemented at the both end of model.

3. RESULTS AND DISCUSSION

3.1 Band Gap Characterization in a Thin Slab with Periodic Pillars Structure

In this section, we discuss the evolution of band gap based on the 2D square lattice system as described in Fig 1(a). The result is presented in Figs. 3(a); a complete band gap between f=312–412 kHz (grey shaded region) was obtained with filling factors, β= 0.502 (where β is defined as β = $\frac{r^2}{a^2}$, where r is the radius of the pillar and a is lattice constant), height of cylinders, h_p= 3.4 mm and thickness of plate, h=1 mm for a unit cell. The band gap can be determined by the two symmetry directions of the square lattice along *ΓX* and *ΓM* directions as illustrated in Figs. 3(b). The scattered waves by the PnC lattice when the wave is spreading was the result for the creation of the Bg.

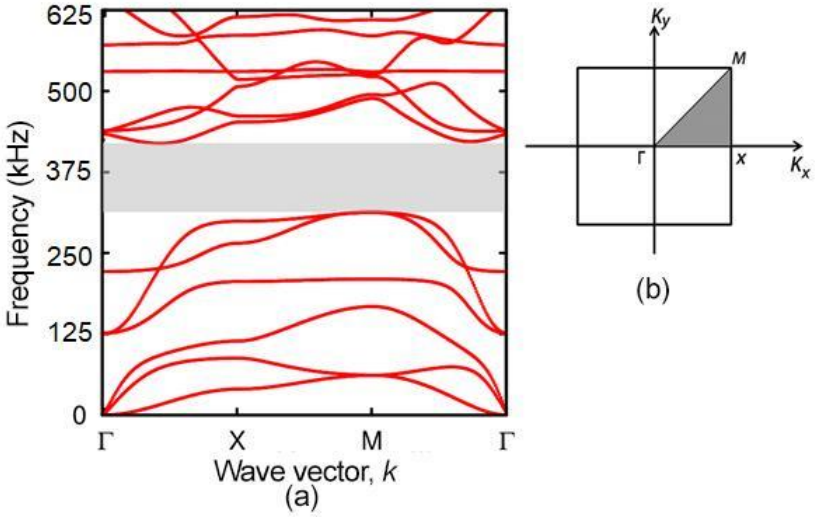

Figure 3. (a) The band dispersion of proposed unit cell in the first irreducible Brillouin zone. The BnG extended from a frequency f=312–412 kHz (b) Brillouin zone of the square lattice unit cell.

We perform several calculations varying in reasonable ranges for the height of pillars, h_p, thickness of slab, h and the pillar radius, r in order to identify the most favorable conditions to obtain the largest band gap. However, in the perspective of a fabrication limitations, we have

limited the radius, r to 1.6 mm, and the height of pillar, h_p to unit. Fig. 4 (a) illustrates the influence of pillars parameter while maintaining the other parameters. We observe two band gaps in Fig. 4 (a) but we exclude the band gap with a weak size of width of the BnG. The remain, shows a BnG for which the width is increases when the h_p increases. Otherwise, we decide to fix the pillar height to 3.4 mm of a as no significant gain which can be obtained with 100% of a. In the same manner, we fix the slab thickness to 1 mm as the width of BnG decreases when the thickness increases (see Fig. 4 (b)). Even though the largest gap is equivalent to 0.6 to 0.8 mm of a, the slab thickness will be too thin and fragile, thus we choose the slab thickness, h= 1 mm. As we increase the thickness of slab, the limits above the BnG are approaching the below limits and reduce the BnG width. In additional, the increase in slab thickness will reduce the resonant coupling between neighbouring pillars and shrink the size of BnG. The slab with thinner dimension simply improves the coupling between pillars and boosting its BnG opening. Furthermore, this opening gap will further improve when the radius of pillars increases. The justification for this is clear since by increasing the radius, r it will reduce the distance between individual pillars and the interaction between localized energy could further improved via surface coupling. As shown in Fig. 4 (c), the BnG opening is gradually increased when the radius increased to justify the claim.

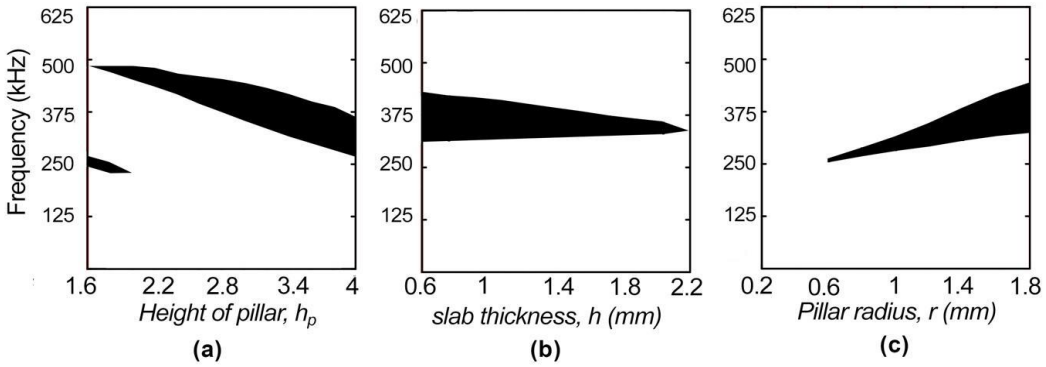

Figure 4. Gap map diagram of frequencies versus normalized (a) height of pillars (b) thickness of slab(c) radius of pillars.

3.2 Propagation in a Linear Defect Phononic Crystal Slab

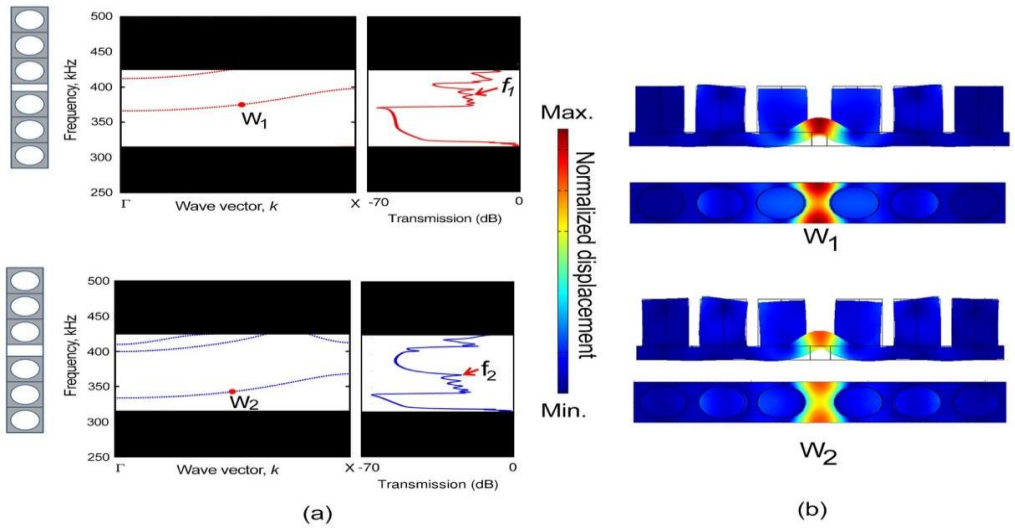

Figure 5. Band diagram and transmission spectra for (a) W_1=1 mm at frequency transmission f = 366-397 kHz and W_2=1.4 mm at frequency transmission f=333-367 kHz (b) total displacement field for waveguide at point W_1 (top) and W_2 (bottom) in (a).

The phononic crystal wave guide can be created by introducing the defect in the perfect crystal structure in which the elastic waves are completely surrounded by the reflecting pillar walls. This linear defect forms a continuous route that enables the energy to fully confined within the defect boundaries and give the possibilities for wave guiding along the pre-defined trajectory. Since the elastic waves can only travel in the defect area and cannot invade into the periodic structures, we expect the presence of localize mode within the complete energy band gap. To interpret this behavior, the supercell technique consists of 7 unit cells with a 4th pillar disturbed was used to understand the property of waveguide dispersion. The waveguide with two defects width, W_1 and W_2 were simulated where W_1 =1 mm and W_2 =1.4 mm is defined as the distance between the defect's width to the neighbouring pillars on the both sides. The displacement fields inside the waveguides are defined and recorded to understand the wave guide properties.

By imposing the selected boundaries as described in sect. 1, the dispersion curve can be plotted to study the behavior of waveguide filtering frequencies. When we introduced the waveguide with defect width W_1 =1 mm, the waveguide extended from k=(0,0) to k=(π,0) that doesn't exist in the perfect crystal appeared within the complete band gap region as depicted in top Fig. 5(a). The filtering frequencies for W_1 =1 mm cover the frequencies f_1 = 366-397 kHz. Similarly, we can create another filtering frequencies for f_2=333-367 kHz by introducing the second waveguides size W_2 =1.4 mm. These two localized modes (f_1 and f_2) are connected to the frequency components of the waveguides and can be transferred to higher or lower frequencies depending on the size of the defect. As we can observe in Fig. 5(a), with the increase of waveguides size from W_1 =1 mm to W_2 =1.4 mm, the transmitting frequency ranges decreased and shifted to lower limits of the band gap. Apparently, the result illustrates the possibility of the structure to be made as elastic wave filter. For instance, the frequency filtration f = 366-397kHz for W_1 can be separated from f=333-367 kHz by including the defect structure W_2. In other words, we can control the wave guide frequency to a desired value with a proper choice of waveguide size.

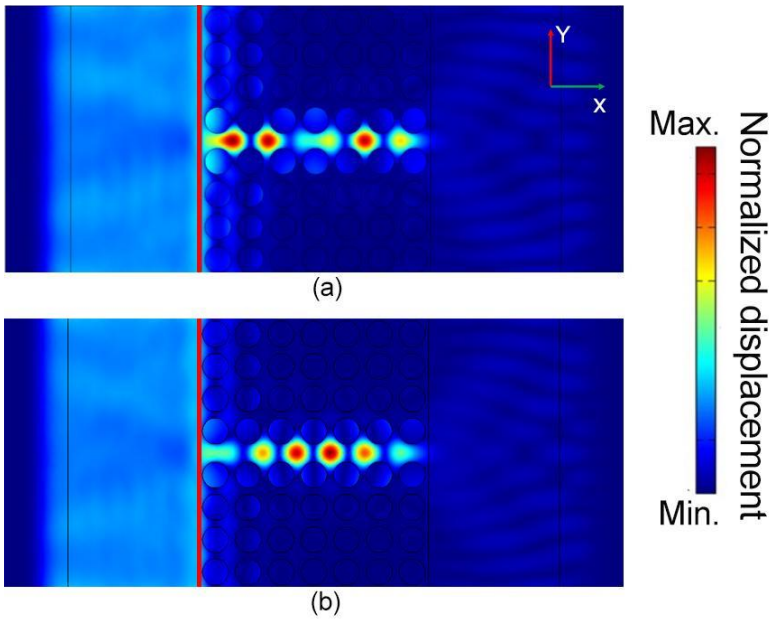

Figure 6. Top view of the surface displacement for (a) W_1=1 mm at transmission frequency f_1=392 kHz (b) W_2=1.4 mm at f_2=368 kHz. The red line indicates the excitation source for the incoming wave.

To understand the trapped wave properties, the displacement for point W_1 and W_2 at k=376 in Fig. 5(a) were calculated and shown in Figs. 5(b) as 3D vector diagram. Both points W_1 and W_2 represents the point frequency at 375 kHz and 343 kHz. The snapshot in Fig. 5(b) illustrates the displacement from the top and side view of waveguide defects with efficient confinement in the guided area without any leaks into adjacent pillars structure. The maximum displacement takes the whole segments of the slab thickness and demonstrate equivalent maximum amplitude in the

upper and bottom side of the slab. Consequently, the slab-based waveguide can undertake any displacement direction i.e., U_x, U_y, U_z with no attenuation issues as in surface acoustic wave (saw) which the maximal amplitude only concentrated on the free surface and decreases exponentially towards the deepest part of the bulk. The calculation for displacement fields in Fig. 5(b) has also showed the confinement has stronger localization energy in narrower corridor size. The maximum displacement with red color indicator can be observed in the displacement field for W_1 =1 mm. Based on the observation on Fig. 5, we observe that the larger waveguide will not only lead to decrease of frequency as observed in the dispersion curve, but also the degree of their displacement confinement. Possibly, this is due to the minimal interruption to the lattice constant of the phononic crystal since an efficient PnC slab waveguide required a very minimal defect size in the crystal.

To illustrate a substantial situation for the actual wave travelling inside the PnC waveguides, Fig 6 shows a 3D linear waveguide structure that shows the surface displacement field for the transmission frequency, f_1 and f_2 in Fig.5(a). The guided wave frequency at f_1=392 kHz for W_1 and f_2=368 kHz for W_2 were generated in the entry of the waveguide row with line extended in the y-direction that covers the boundaries of pillar inclusion. The out-of-plane displacement, U_z component are presented in color bar spectrum with the minimum displacements is represented in dark blue and the maximum displacement in dark red spectrum. For amenity, the scale is fixed and normalized to observe the correlation of amplitude for different cases. Results show the guided waves are confined well within the defect rows with minimum leakage into the periodic inclusion boundary. But the energy leakage is negligible because the waveguide channel are capable of carrying most of the energy along the guided route.

4. CONCLUSION

The propagation of elastic waves in phononic crystal slabs composed of square lattice array of nickel embedded in lithium niobate has been studied theoretically. The dispersion curve and the transmission spectra are theoretically calculated with Finite Element Methods (FEM) and represents a complete band gap ranging from f=312–412 kHz frequency. With a proper choice of geometrical and physical properties of materials, a complete band gap for an elastic wave can be optimized. We demonstrated the ability of linear defect structure in the periodic pillars to confine an elastic wave for wave guiding application. From the observation, one can design a passive device in which the defect distance in the crystal phononic lattice could play a central role to avoid or permit any transmission of elastic waves frequencies pass band along the selective waveguide.

ACKNOWLEDGEMENTS

This work has been supported by the research grant GUP-2019-070. The author would like to extend gratitude to Skim Zamalah Penyelidik Tersohor from CRIM, Universiti Kebangsaan Malaysia.

REFERENCES

[1] Tanaka, Y., Tomoyasu, Y., Tamura, S., Phys Rev B **62**, 11 (2000) 7387-7392.
[2] Kushwaha, M. S., Halevi, P., Martinez, G., Dobrzynski, L., Djafari-Rouhani, B., Phys Rev B **49**, 4 (1994) 2313-2322
[3] Vasseur, J. O., Djafari-Rouhani, B., Dobrzynski, L., Kushawa, M. S., Halevi, P., J. of Phys: Condens. Matter, **6**, 42 (1994) 8759-8770.
[4] Kuang, W., Hou, Z., Liu, Y., Phys Lett A **332**, 5-6 (2004) 481-490
[5] Wu, T.T., Huang, Z-G, Lin, S., Phys Rev B **69**, 9 (2004) 094301

[6] Pennec, Y., Djafari-Rouhani, B., Vasseur, J., Khelif, A., Deymier, P.A., Physical Review E **69**, 4 (2004) 046608.
[7] Rostami-Dogolsara, B., Moravvej-Farshi, M. K., Nazari, F., Journal of Molecular Liquids **281** (2019) 100-107.
[8] Kadmiri, I. E., Ben-Ali, Y., Khaled, A., Bria, D., "Y-shaped branch structure using asymmetric resonators for phononic demultiplexing." in Materials Today: Proceedings, (2020).
[9] Wang, Y., Lee, J., Zheng, X-Q., Xie, Y., Feng, P. X.-L., ACS Photonics **6**, 12 (2019) 3225-3232.
[10] Motaei, F., Bahrami, A., Physica Scripta **9**, 6 (2020) 065703
[11] Motaei, F., Bahrami A., Photonics and Nanostructures Fundamentals and Applications **39** (2020) 100765.
[12] Wu, T. C., Wu, T. T., Hsu, J. C., Physical Review B **79**, 10 (2009) 104306.
[13] Olsson, R. H., El-Kady, I. F., Su, M. F., Tuck, M.R., Fleming, J. G., Sensors and Actuators A: Physical **145-146** (2008) 87–93.
[14] Mohammadi, S., Eftekhar, A. A., Hunt, W. D., Adibi, A., Applied Physics Letters **94** (2009) 051906.
[15] Oudich, M., Assouar, M. B., Hou, Z., Applied Physics Letters. **97** (2010) 193503.
[16] Vasseur, J. O., Deymier, P. A., Djafari-Rouhani, B., Pennec, Y., Hladky-Hennion, A.-C., Physical Review B **77**, 8 (2008) 085415.
[17] Khelif, A., Choujaa, A., Benchabane, S., Djafari-Rouhani, B., Laude, V., Applied Physics Letters **84**, 22 (2004) 4400–4402.
[18] Miyashita, T., Meas. Sci. Technol. **16**, 5 (2005) R47-R63.
[19] A. Khelif, A. Adibi, Phononic Crystals: Fundamental and Applications, Ed. New York; Springer, (2016) 113
[20] Khelif, A., Choujaa, A., Benchabane, S., Djafari-Rouhani, B., Laude, V., Applied Physics Letters, **84**, 22 (2004) 4400-4402.
[21] K-Y. Hashimoto, RF bulk acoustic wave filters for communications; Artech House, (2009) 111
[22] Addouche, M., Al-Lethawe, M. A., Elayouch, A., Khelif, A., AIP Advances **4**, 12 (2014) 124303.